Acta Crystallographica Section D
Biological Crystallography
ISSN 0907-4449

pH-tuneable binding of 2′-phospho-ADP-ribose to ketopantoate reductase: a structural and calorimetric study

Alessio Ciulli,[a] Carina M. C. Lobley,[b] Kellie L. Tuck,[a]‡ Alison G. Smith,[c] Tom L. Blundell[b] and Chris Abell[a]*

[a]University Chemical Laboratory, Lensfield Road, Cambridge CB2 1EW, England, [b]Department of Biochemistry, University of Cambridge, 80 Tennis Court Road, Cambridge CB2 1GA, England, and [c]Department of Plant Sciences, University of Cambridge, Downing Street, Cambridge CB2 3EA, England

‡ Present address: School of Chemistry, Monash University, Australia.

Correspondence e-mail: ca26@cam.ac.uk

Received 5 October 2006
Accepted 25 October 2006

PDB Reference: ketopantoate reductase–2′-monophospho-adenosine 5′-diphosphoribose complex, 1yon, r1yonsf.

The crystal structure of *Escherichia coli* ketopantoate reductase in complex with 2′-monophosphoadenosine 5′-diphosphoribose, a fragment of $NADP^+$ that lacks the nicotinamide ring, is reported. The ligand is bound at the enzyme active site in the opposite orientation to that observed for $NADP^+$, with the adenine ring occupying the lipophilic nicotinamide pocket. Isothermal titration calorimetry with R31A and N98A mutants of the enzyme is used to show that the unusual 'reversed binding mode' observed in the crystal is triggered by changes in the protonation of binding groups at low pH. This research has important implications for fragment-based approaches to drug design, namely that the crystallization conditions and the chemical modification of ligands can have unexpected effects on the binding modes.

1. Introduction

Ketopantoate reductase (KPR; EC 1.1.1.169), an enzyme involved in the biosynthesis of pantothenate (vitamin B_5), catalyses the reduction of ketopantoate to form pantoate using NADPH as a cofactor (Ciulli & Abell, 2005). The enzyme from *Escherichia coli*, encoded by the *panE* gene, has been purified and extensively characterized both biochemically (Zheng & Blanchard, 2000*a*,*b*, 2003) and structurally (Matak-Vinkovic *et al.*, 2001; Lobley *et al.*, 2005). The crystal structure of the apoenzyme was solved at 1.70 Å resolution using the selenomethionine MAD method (Matak-Vinkovic *et al.*, 2001). KPR belongs to the 6-phosphogluconate dehydrogenase superfamily in the SCOP database (Murzin *et al.*, 1995) and has properties of both class A and class B secondary alcohol dehydrogenases (Zheng & Blanchard, 2000*a*). The secondary structure comprises 15 α-helices and 11 β-strands. The enzyme is monomeric and has two domains separated by the active-site cleft. The N-terminal domain has the $\alpha\beta$ Rossmann-type fold featured in many nucleotide-binding proteins, with a glycine-rich region (^{7}GCGALG^{12}) for nucleotide recognition, whilst the C-terminus is an α-helical domain. We have also solved the crystal structure of KPR in complex with $NADP^+$ (Lobley *et al.*, 2005). This structure showed the cofactor bound in an extended conformation in the cleft between the two domains and identified the interactions formed with key residues at the enzyme active site (Lobley *et al.*, 2005). More recently, a systematic biophysical analysis was conducted to probe hot spots at the cofactor-binding site using a series of $NADP^+$ fragments and analogues (Ciulli *et al.*, 2006). There is a conservation of the NADP-like binding mode across the series of fragments. The 2′-phosphate and the reduced nicotinamide are key binding groups for cofactor recognition (Ciulli *et al.*, 2006).

Table 1
Statistics of KPR data collection and refinement.

Values in parentheses are for the outer shell.

Data collection	
X-ray source	ESRF (14-4)
Space group	$P2_12_12_1$
Unit-cell parameters (Å, °)	$a = 60.32$, $b = 65.83$, $c = 98.21$, $\alpha = \beta = \gamma = 90$
Wavelength (Å)	0.939
Resolution range (Å)	50–1.95 (2.0–1.95)
No. of unique reflections	28985
Multiplicity	7.3
$R_{\rm merge}$	11.5 (47.6)
Average $I/\sigma(I)$	23.2 (2.6)
Reflections with $I/\sigma(I) > 3$ (%)	79.2 (10.6)
Completeness (%)	99.2 (92.7)
Mosaicity (°)	0.70
Wilson B (Å^2)	28.2
Refinement	
$R_{\rm cryst}$† (%)	16.6
$R_{\rm free}$‡ (%)	19.4
No. of reflections in working set	27446
No. of reflections in test set	1471
No. of residues rebuilt	292
Model quality	
Estimated coordinate error§ (Å^2)	1.27
Ramachandran plot¶	
Most favoured (%)	98.6
Generously allowed (%)	1.4
Disallowed (%)	0
R.m.s.d. bonds (Å)	0.02
R.m.s.d. angles (°)	1.8
Overall mean B (Å^2)	31.1

† $R_{\rm cryst} = \sum ||F_{\rm obs}| - |F_{\rm calc}|| / \sum |F_{\rm obs}|$, where $F_{\rm obs}$ and $F_{\rm calc}$ are the observed and calculated structure-factor amplitudes. ‡ $R_{\rm free}$ as for $R_{\rm cryst}$ using a random subset of data excluded from the refinement. § Estimated coordinate error based on the free R value as calculated by *REFMAC* (Collaborative Computational Project, Number 4, 1994; Murshudov *et al.*, 1997). ¶ Calculated using *RAMPAGE* (Lovell *et al.*, 2003).

In this paper, we report the three-dimensional structure of KPR in complex with 2′-monophosphoadenosine 5′-diphosphoribose (2′P-ADP-ribose), a fragment of NADPH that lacks the nicotinamide ring, solved to 1.95 Å resolution. The structure surprisingly reveals the ligand to be bound in the opposite orientation to that observed for NADP$^+$, with the adenine ring occupying the lipophilic nicotinamide pocket. Detailed analysis of this unexpected crystallographic result using isothermal titration calorimetry (ITC) and site-directed mutagenesis revealed that this unusual 'reversed binding mode' is triggered by changes in the protonation of binding groups at low pH.

2. Experimental

2.1. Protein expression, purification and site-directed mutagenesis

For ITC studies, wild-type (WT) KPR and site-directed mutants of KPR were expressed with an N-terminal His$_6$ tag, whereas WT KPR for crystallization studies had no tag. Both constructs were expressed and purified as described previously (Lobley *et al.*, 2005; Ciulli *et al.*, 2006). Purified His$_6$-tagged protein was dialyzed into the appropriate buffer using Slide-A-Lyzer dialysis cassettes (Pierce). The protein concentration was determined from the A_{280}, using an absorption coefficient for His$_6$-KPR of 62 650 M^{-1} cm^{-1} determined from amino-acid analysis [Protein and Nucleic Acid Chemistry Facility (PNAC), Cambridge]. An absorption coefficient of 47 870 M^{-1} cm^{-1} estimated from the sequence was used for untagged KPR. The genes for the singly mutated forms of KPR, R31A and N98A were made using the QuickChange Site-Directed Mutagenesis Kit (Stratagene) as described previously (Ciulli *et al.*, 2006).

2.2. Crystallization of KPR

Crystallization trials were carried out using the hanging-drop vapour-diffusion method as described previously (Lobley *et al.*, 2005). Prior to crystallization, KPR samples (10–15 mg ml^{-1}) were incubated at 277 K with NADPH and pantoate at a final ligand:protein ratio of 2:1 and 5:1, respectively. Needle-like crystals of KPR were obtained in 10% 2-methyl-2,4-pentanediol (MPD) buffered with 0.1 *M* sodium acetate pH 4.0–5.0. Crystals were cryoprotected in 30% MPD buffered with 0.1 *M* sodium acetate at the same pH as the well solution. Attempts to crystallize KPR at a pH close to 7 were unsuccessful.

2.3. X-ray data collection, crystal structure determination and refinement

X-ray data were collected to 1.95 Å resolution at station 14.4, European Synchrotron Radiation Facility. The principal parameters and data statistics for this data collection are shown in Table 1. *DENZO* and *SCALEPACK* from the *HKL*-2000 suite were used to process and scale the data (Otwinowski & Minor, 1997). The structure was solved using molecular replacement, with apo KPR as the probe structure. *AMoRe* from the *CCP*4 suite (Collaborative Computational Project, Number 4, 1994; Navaza, 1994, 2001) was used for molecular replacement. After molecular replacement, the initial model underwent simulated annealing using *CNS* (Brünger *et al.*, 1998) and initial electron-density maps were generated. Refinement involved an iterative cycle of manual rebuilding in *XTALVIEW* (McRee, 1999) and maximum-likelihood refinement using *REFMAC*5 from the *CCP*4 suite (Murshudov *et al.*, 1997; Collaborative Computational Project, Number 4, 1994). The completed structure is of residues 1–292 of KPR in complex with one molecule of 2′P-ADP-ribose. Nonprotein molecules were obtained from the HIC-Up database (Kleywegt & Jones, 1998) and refinement libraries were taken from the *PRODRG* server (Schüttelkopf & van Aalten, 2004).

2.4. Stability analysis of NADP(H)

The stability of NADPH and NADP$^+$ were investigated at pH 5. 1.5 mg NADPH and 1.5 mg NADP$^+$ were dissolved in 700 µl 0.1 *M* sodium acetate pH 5. NMR spectra were recorded at 0, 2, 4, 24 and 48 h time intervals at 298 K on a Bruker DRX 500 MHz spectrometer equipped with a 5 mm triple-resonance inverse (TXI) cryoprobe with Z-gradients using a presaturation pulse sequence. Mass spectrometry was

carried out using a Micromass Quadrupole–Time of Flight (Q-TOF) spectrometer. The degradation product of NADPH was identified by mass spectrometry to be 2′P-ADP-ribose: m/z ($C_{15}H_{25-n}N_5Na_nO_{17}P_3$) = 727.96 ($n$ = 4, MH^+, 90%), 705.98 (n = 3, 100%), 684.00 (n = 2, 45%).

2.5. Isothermal titration calorimetry

ITC experiments were performed on an OMEGA isothermal titration calorimeter from Microcal Inc. at 300 K. Purified protein was exhaustively dialyzed with 0.1 *M* HEPES pH 7.7 and loaded into the sample cell at a final concentration of 30–80 µ*M*. Sufficient ligand was used to obtain at least 80% saturation of the enzyme at the end of the titration, as estimated using the equation given by Turnbull & Daranas (2003). Typically, 35 injections of 7–8 µl were made at 3–4 min intervals from a 300 µl syringe rotating at 300 rev min^{-1}. Alternatively, the initial 15 injections were of 3–4 µl and the final 30 injections were of 7–8 µl, all at 3–4 min intervals. The heat change accompanying the titration was recorded as differential power by the instrument and determined by integration of the peak obtained. Titrations of ligands to buffer only were performed to allow baseline corrections. The corrected heat change was then fitted using nonlinear least-squares minimization to obtain the dissociation constants K_d, the enthalpy of binding ΔH and the stoichiometry n (Wiseman *et al.*, 1989). A stoichiometry of 1, determined from titrations with $NADP^+$ under a high c value, was fixed during curve fitting of data obtained with 2′P-ADP-ribose under low c-value conditions (Ciulli *et al.*, 2006). At least two experiments were performed at different ligand concentrations to exclude the occurrence of any concentration-dependent phenomena.

3. Results and discussion

3.1. Crystallization, structure solution and refinement

In an attempt to crystallize the ternary complex between KPR, NADPH and pantoate, we explored conditions similar to those used for the KPR–$NADP^+$ crystals (Lobley *et al.*, 2005) and obtained crystals at pH 4.0–5.0. Molecular replacement using *AMoRe* (Collaborative Computational

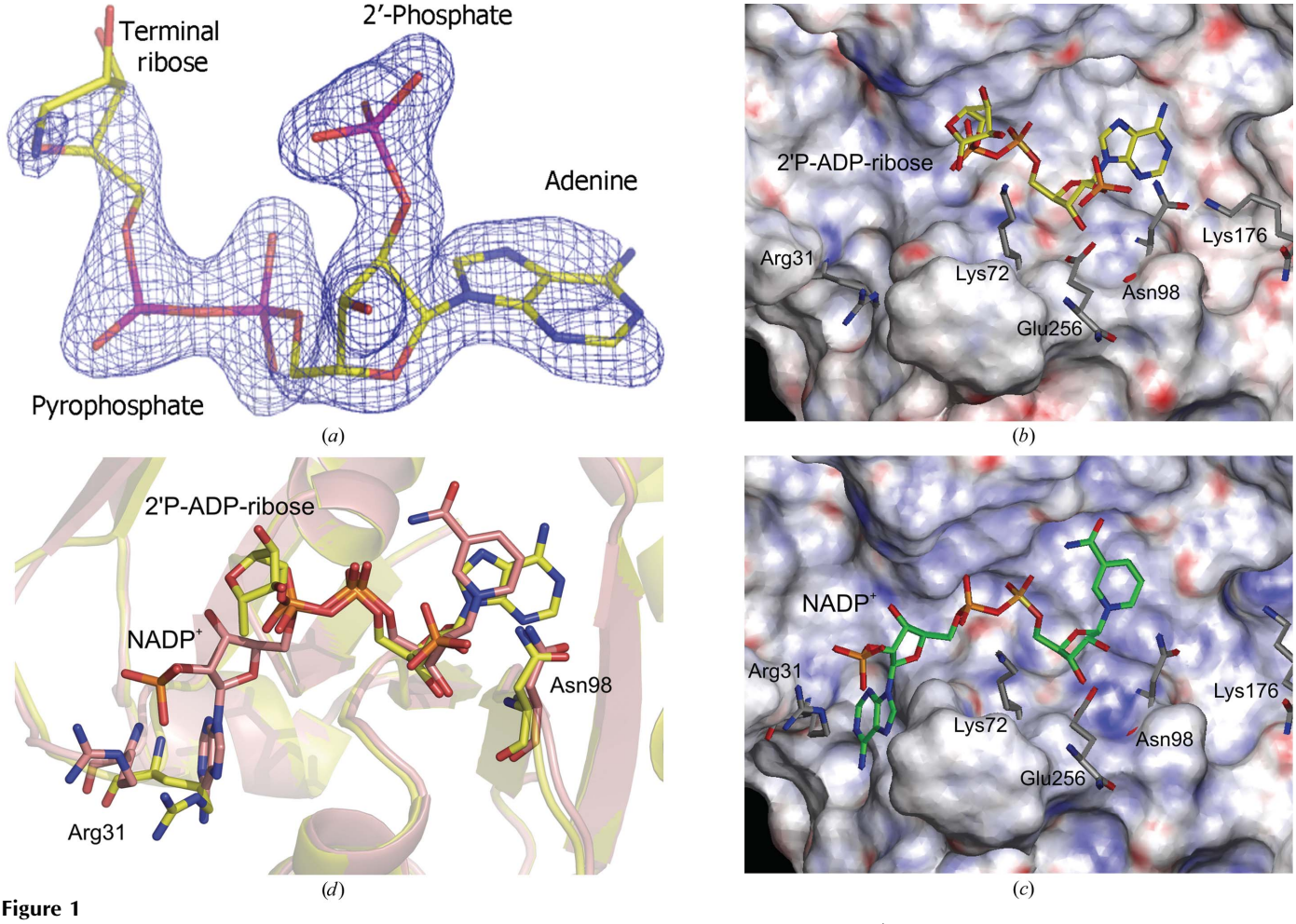

Figure 1
Crystal structure of the KPR–2′P-ADP-ribose binary complex and comparison with the KPR–$NADP^+$ complex. (*a*) 2′P-ADP-ribose electron density. The final $2F_o - F_c$ electron-density map for 2′P-ADP-ribose contoured at 1σ is shown in blue. Binding modes of (*b*) 2′P-ADP-ribose and (*c*) $NADP^+$ and the key residues at the active site of KPR are shown. The van der Waals surface of the N-terminal domain (residues 1–176) only is shown, coloured by electrostatic potential (neutral, white; positive, blue; negative, red). (*d*) Superposition of the KPR–$NADP^+$ (salmon pink) and KPR–2′P-ADP-ribose (yellow) structures. The protein structures were superposed using the backbone atoms of residues 2–291.

Project, Number 4, 1994; Navaza, 1994, 2001) with apo KPR (Matak-Vinkovic *et al.*, 2001) as the probe structure gave a solution with an R_{cryst} of 21.2% and a correlation coefficient of 55.7%. Initial $2F_o - F_c$ and $F_o - F_c$ electron-density maps clearly showed the presence of a nonprotein molecule in the active site. However, no electron density corresponding to pantoate was identified; instead, it was possible to fit the density corresponding to part of NADPH. Ultimately, one molecule of 2′P-ADP-ribose was built into this density (Fig. 1*a*). Although electron density is incomplete for the terminal ribose, the presence of final $2F_o - F_c$ electron density at 3–5σ around the phosphate groups gave a clear indication of the position of the ligand and enabled its unambiguous modelling. Maximum-likelihood refinement implemented in *REFMAC*5 (Murshudov *et al.*, 1997) was used to improve the quality of the electron-density maps and facilitate further rebuilding and improvement of the molecular model until no unexplained electron density remained and the R_{cryst} and R_{free} values converged at 16.6 and 19.4%, respectively (Table 1). As in the apo (Matak-Vinkovic *et al.*, 2001) and holo (Lobley *et al.*, 2005) structures, the C-terminal residues were disordered and nine residues were not rebuilt.

3.2. Identification of 2′P-ADP-ribose as the degradation product of NADPH

The most likely source of 2′P-ADP-ribose in the structure was as a result of degradation of the NADPH used in the cocrystallization experiments. NADPH is known to be an inherently unstable compound (Burton & Kaplan, 1963; Lowry *et al.*, 1961). The hydrolysis of NADPH to 2′P-ADP-ribose has previously been observed in crystals of acetohydroxyacid isomeroreductase grown in the presence of NADPH (Thomazeau *et al.*, 2000).

We monitored the stability of NADPH and $NADP^+$ at pH 5 using NMR spectroscopy to confirm the degradation of NADPH to 2′P-ADP-ribose under the crystallization conditions. Several NMR spectra were acquired over 48 h. At pH 5, NADPH degraded completely within 4 h, whereas $NADP^+$ did not show any degradation. The degradation of NADPH could be monitored by following the disappearance of the resonances at δ 2.7 (2H, H4, nicotinamide ring), δ 6.0 (1H, H6, nicotinamide ring) and δ 7.0 (1H, H2, nicotinamide ring). The disappearance of these peaks corresponded to the appearance of a doublet at δ 5.5, which is indicative of the formation of 2′P-ADP-ribose.

Mass-spectrometry experiments were used to confirm the formation of 2′P-ADP-ribose upon incubation of NADPH at pH 5. The peak observed at 728 Da corresponds to the calculated weight of the protonated 2′P-ADP-ribose tetrasodium salt. These measurements confirmed the hydrolysis of NADPH to 2′P-ADP-ribose.

3.3. The structure of the binary complex of KPR with 2′P-ADP-ribose

2′P-ADP-ribose binds to KPR in the active-site cleft between the N-terminal Rossmann-fold domain and the C-terminal α-helical domain. The adenine ring of 2′P-ADP-ribose hydrogen bonds to the main-chain amide and carboxyl of Thr118, the 2′-phosphate makes hydrogen bonds to Glu256 and Ser244, Asn98 binds the ribose O2 and O3 atoms and provides part of the adenine pocket, the remaining part being formed by the hydrophobic side chains of Leu11 and Ile96, and the pyrophosphate makes hydrogen bonds with backbone amide NH groups of Ala10 and Leu11 and with a structurally conserved water molecule at the ^{7}GCGALG^{12} glycine-rich loop (Bottoms *et al.*, 2002). There is relatively poor electron density in the region corresponding to the terminal ribose (see Fig. 1*a*), suggesting that the binding of the ribose moiety may be disordered.

The adenine recognition in the structure presented here can be related to the adenine-binding motif described by Denessiouk *et al.* (2001). In this recognition motif, which is common to many enzymes that bind adenine cofactors, an amino acid forms hydrogen bonds to the N1 nitrogen and the NH_2 group of adenine with its backbone amide NH and carbonyl groups, respectively. Here this residue is Thr118, which forms two hydrogen bonds of 3.2 and 2.6 Å, respectively. The hydrophobic side chains of Leu11 and Ile96 are positioned below the plane of the adenine ring, which is another common feature of the adenine-recognition motif.

3.4. Comparison with the KPR–$NADP^+$ binary complex structure

A comparison of the KPR–$NADP^+$ and KPR–2′P-ADP-ribose structures is shown in Figs. 1(*b*), 1(*c*) and 1(*d*). Previous biophysical studies identified the adenosyl-2′-phosphate pocket and the nicotinamide pocket for NADPH as two distinct hot spots for ligand binding (Ciulli *et al.*, 2006). In the KPR–$NADP^+$ binary structure, both pockets are occupied by the cofactor molecule (Fig. 1*c*). However, in the KPR–2′P-ADP-ribose binary structure only one pocket is occupied. Here, the adenine group of 2′P-ADP-ribose occupies the apolar nicotinamide pocket (Fig. 1*b*), whilst no electron density was found for binding in the adenosyl-2′-phosphate pocket. The ligand is consequently bound in the opposite orientation to $NADP^+$ and we henceforth refer to this as the 'reversed binding mode'. Closer inspection shows that many of the interacting residues, *e.g.* Lys72, Asn98 and Glu256, are common to both modes of binding (Figs. 1*b* and 1*c*). Superposition of the two crystal structures reveals that the adenine ring of 2′P-ADP-ribose is almost coplanar with the nicotinamide ring of $NADP^+$ and the pyrophosphate groups from each structure overlap well (Fig. 1*d*).

There are two notable differences in the active-site cleft of KPR–2′P-ADP-ribose when compared with KPR–$NADP^+$. Firstly, the side chain of Arg31 moves towards Trp74 and Gln75 in order to close the gap left by the absence of cofactor in the adenine-binding pocket. Secondly, the side chain of Lys176 points in the direction of the adenine ring (Fig. 1*b*) rather than being involved in a hydrogen bond to Thr117 as in the KPR–$NADP^+$ complex. Interestingly, in the KPR–2′P-ADP-ribose structure Lys176 adopts the conformation

proposed for binding ketopantoate in the KPR–NADPH–ketopantoate ternary complex model (Lobley *et al.*, 2005).

3.5. Comparison with acetohydroxyacid isomeroreductase crystal structures

Acetohydroxyacid isomeroreductase (AHIR; EC 1.1.1.86) catalyses the conversion of acetohydroxy acid into dihydroxyvalerate using NADPH as cofactor, which is the second step in the biosynthetic pathway to the branched side-chain amino acids valine, leucine and isoleucine (Biou *et al.*, 1997). It is known that AHIR can catalyze the same reaction as KPR (Primerano & Burns, 1983; Matak-Vinkovic *et al.*, 2001). In a recently published crystal structure of AHIR (PDB code 1qmg), crystallization was carried out in the presence of NADPH and the substrate 2-aceto-2-hydroxybutyrate at pH 7.2 (Thomazeau *et al.*, 2000). Instead of NADPH, 2′P-ADP-ribose was bound in the active site, which was also shown to be a result of cofactor degradation (Thomazeau *et al.*, 2000). However, in this structure 2′P-ADP-ribose was bound in the same conformation as NADPH, as had been previously seen in the crystal structure of the AHIR–NADPH complex (PDB code 1yve; Biou *et al.*, 1997), which was also obtained at pH 7.2.

The observation of the two different binding orientations for 2′P-ADP-ribose in AHIR and KPR was unexpected. However, the conditions under which the two proteins were crystallized were not identical and specifically the pH was quite different. The crystallization conditions for KPR were at a pH between 4.0 and 5.0, whereas those for AHIR were at pH 7.2. Furthermore, recent biophysical studies of KPR with cofactor fragments have shown that 2′P-ADP-ribose adopts the same binding mode as $NADP^+$ at physiological pH (Ciulli *et al.*, 2006). Therefore, it was considered possible that the difference in pH was giving rise to the reversed binding mode observed in the KPR complex. There is precedent for protein crystallization conditions, particularly pH, having a pronounced effect on the binding mode of a ligand (Davis *et al.*, 2003). To resolve this issue, the binding interaction of KPR

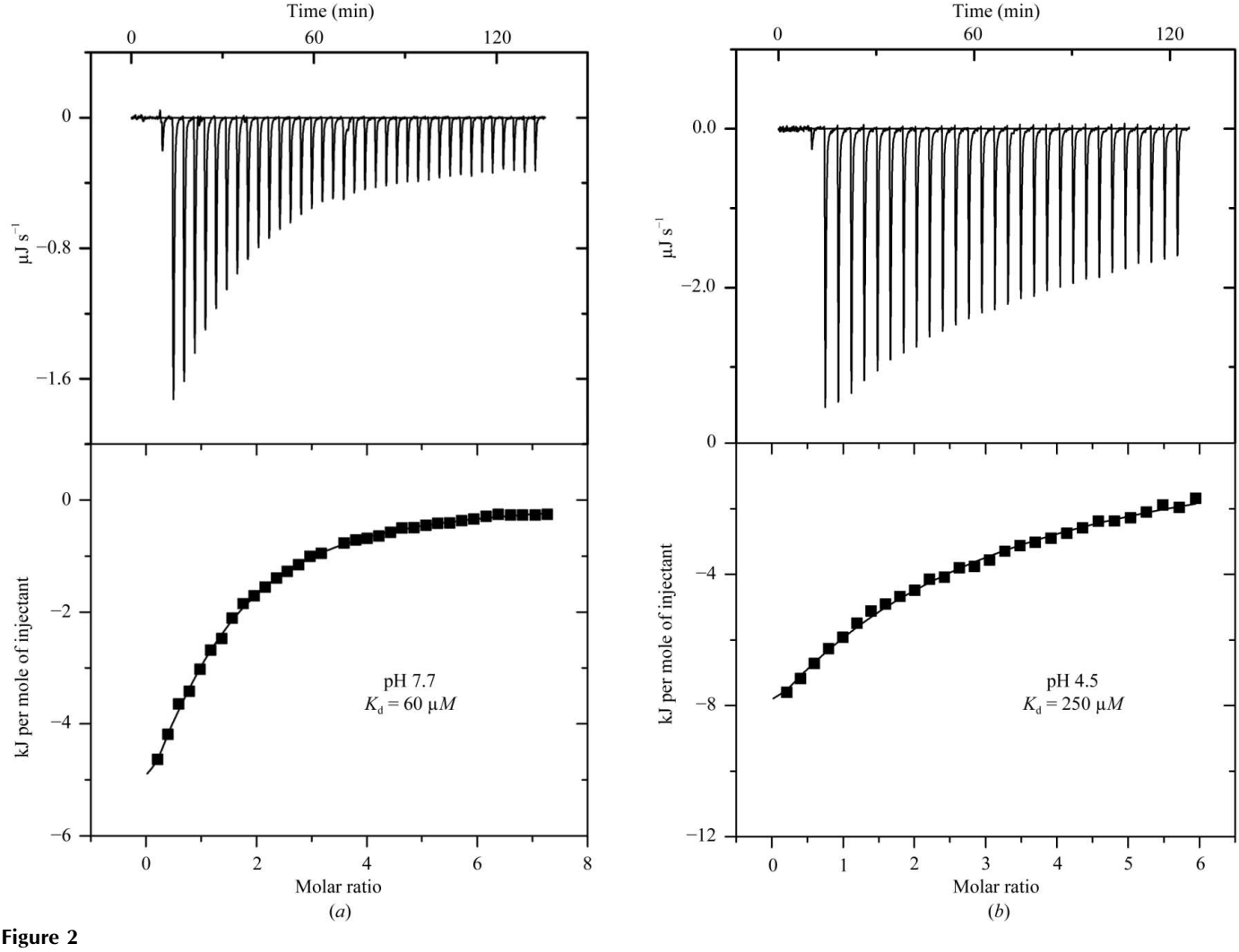

Figure 2
ITC analysis of 2′P-ADP-ribose binding to KPR at different pH values. ITC experiments are shown for His_6-KPR titrated with 2′P-ADP-ribose at 300 K in (*a*) 0.1 *M* HEPES–HCl pH 7.7 and (*b*) 90 m*M* sodium acetate, 5 m*M* HEPES pH 4.5. Top panels: raw data for titrations of 1–2 m*M* ligand into 30–60 μ*M* protein. Each peak corresponds to one injection. An initial 1 μl injection was followed by 35 × 8 μl (*a*) or 28 × 10 μl injections (*b*). Bottom panel: integration of the data, corrected for the heat of dilution. The line represents the least-squares fit to the single-site binding model by the *Origin* program.

with NADP$^+$ and 2′P-ADP-ribose were investigated under different pH conditions using ITC.

3.6. Isothermal titration calorimetry

ITC studies have been previously conducted with substrates (Lobley *et al.*, 2005), cofactors and cofactor analogues (Ciulli *et al.*, 2006; Ciulli & Abell, 2005) binding to KPR at pH 7.7. Titrations of His_6-KPR with 2′P-ADP-ribose were repeated at pH 4.5 under conditions similar to those of crystallization. Typical ITC traces are shown in Fig. 2. Similar experiments were also conducted with NADP$^+$ as reference. The thermodynamic parameters of the interactions were characterized (Table 2) and compared with those determined at pH 7.7. The dissociation constant of NADP$^+$ at pH 4.5 was 100 μ*M*, an increase of 17-fold relative to pH 7.7 (Table 2). In contrast, 2′P-ADP-ribose was found to bind only four times more weakly at pH 4.5 (K_d = 250 μ*M*) than at pH 7.7. Moreover, the relative enthalpic and entropic contributions to affinity changed significantly in the case of the fragment, with a large negative ΔH of -51.1 kJ mol^{-1} at pH 4.5 compared with a ΔH of -12.6 kJ mol^{-1} observed at pH 7.7. Large changes in ΔH often indicate a change in binding mode (Ward & Holdgate, 2001; Holdgate & Ward, 2005).

3.7. Calorimetric analysis of the effect of R31A and N98A mutations

ITC binding studies suggested a change in the binding mode of 2′P-ADP-ribose with pH. To provide additional structural evidence for the proposed changes, single point mutations of Arg31 and Asn98 to Ala were constructed. Mutants R31A and N98A of His_6-KPR had been previously used to probe fragment binding and locate the site of interaction (Ciulli *et al.*, 2006).

Titrations of 2′P-ADP-ribose and NADP$^+$ against the R31A and N98A mutants of KPR were conducted at pH 4.5 using ITC under the same conditions used for the WT enzyme and were compared with those obtained at pH 7.7 (Ciulli *et al.*, 2006). Thermodynamic data for the KPR mutants relative to WT are reported in Table 3 as $\Delta\Delta G$ ($\Delta G_{mutant} - \Delta G_{WT}$) together with the relative contributions from $\Delta\Delta H$ ($\Delta H_{mutant} - \Delta H_{WT}$) and $-T\Delta\Delta S$ [$-T(\Delta S_{mutant} - \Delta S_{WT})$]. At pH 7.7, the effects of both mutations on 2′P-ADP-ribose binding are consistent with those on NADP$^+$ binding, suggesting that the fragment adopts the same binding mode of NADP$^+$. In particular, the side chain of Arg31 appears to be crucial for ligand recognition by binding

Table 2
Thermodynamic parameters of nucleotide binding to *E. coli* KPR.

Errors quoted are standard deviations from multiple experiments.

Ligand	K_d (μ*M*)	ΔG (kJ mol^{-1})	ΔH (kJ mol^{-1})	$-T\Delta S$ (kJ mol^{-1})
pH 7.7†				
NADP$^+$	5.8 ± 0.8	−30.2 ± 0.3	−13.4 ± 0.4	−17.2 ± 0.4
2′P-ADP-ribose	61 ± 8	−24.3 ± 0.3	−12.6 ± 1.3	−11.7 ± 1.7
pH 4.5‡				
NADP$^+$	100 ± 4	−23.1 ± 0.1	−7.1 ± 2.1	−16.0 ± 2.1
2′P-ADP-ribose	250 ± 65	−20.8 ± 0.7	−51.1 ± 3.8	30.1 ± 4.6

† From Ciulli *et al.* (2006). ITC titrations were performed in 0.1 *M* HEPES–HCl pH 7.7 at 300 K. ‡ ITC titrations were performed in 90 m*M* sodium acetate, 5 m*M* HEPES–HCl pH 4.5 at 300 K.

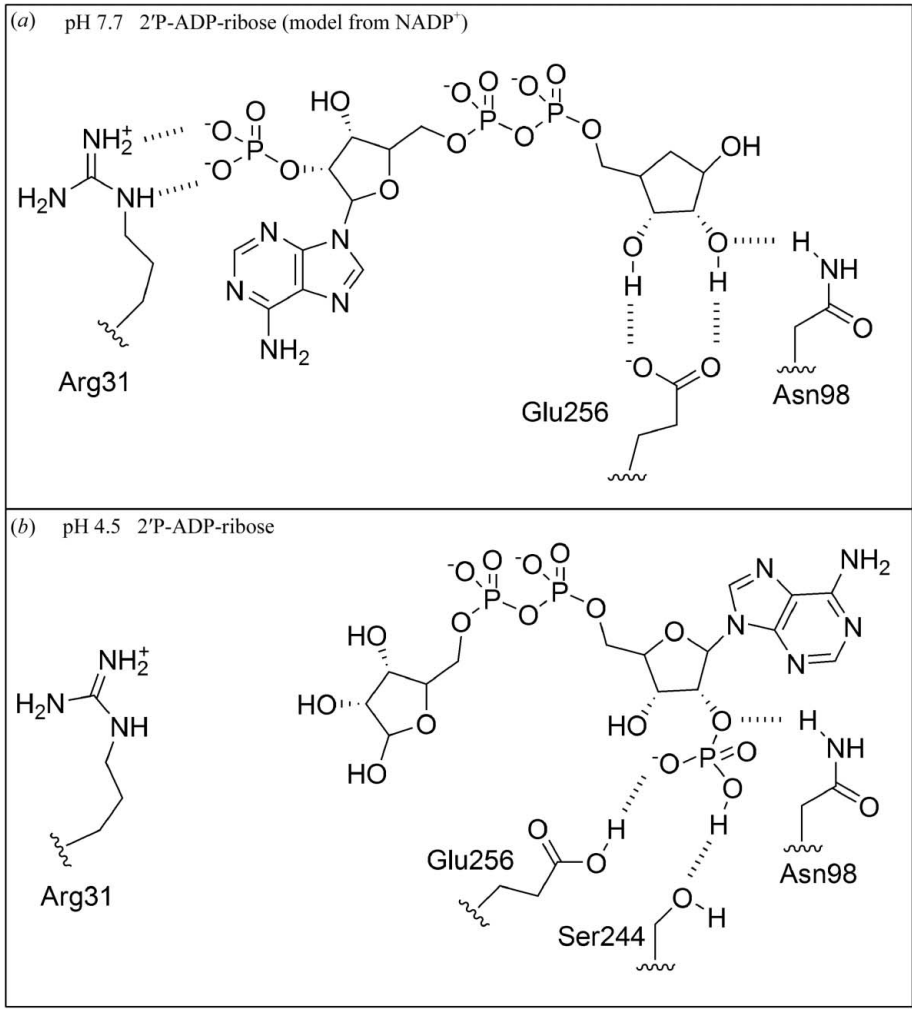

Figure 3
Changes in protonation states tune the binding mode of 2′P-ADP-ribose. (*a*) At pH 7.7 both the 2′-phosphate group of the ligand and Glu256 will be negatively charged, carrying a −2 and a −1 charge, respectively. Their interaction would be highly unfavourable. The ligand binds in the same orientation observed for NADP$^+$, anchoring the 2′-phosphate close to Arg31 and hydrogen bonding to Glu256 *via* the terminal ribose. (*b*) Binding mode observed in the KPR–2′P-ADP-ribose crystal structure reported here. At pH 4.5 the 2′-phosphate becomes protonated (pK = 6.5) carrying a single negative charge. Glu256 is likely to protonate, allowing a favourable hydrogen bond to the 2′-phosphate group.

Table 3
Effect of point mutations on the thermodynamic parameters of nucleotide binding.

$\Delta\Delta G$, $\Delta\Delta H$ and $-T\Delta\Delta S$ are $\Delta G_{mutant} - \Delta G_{WT}$, $\Delta H_{mutant} - \Delta H_{WT}$ and $-T(\Delta S_{mutant} - \Delta S_{WT})$, respectively. n.d., not determined.

	R31A			N98A		
	$\Delta\Delta G$ (kJ mol^{-1})	$\Delta\Delta H$ (kJ mol^{-1})	$-T\Delta\Delta S$ (kJ mol^{-1})	$\Delta\Delta G$ (kJ mol^{-1})	$\Delta\Delta H$ (kJ mol^{-1})	$-T\Delta\Delta S$ (kJ mol^{-1})
pH 7.7†						
NADP$^+$	6.7	3.8	2.9	−6.3	−8.4	2.1
2′P-ADP-ribose	8.8	n.d.	n.d.	−2.5	−9.6	7.1
pH 4.5‡						
NADP$^+$	>6.3	n.d.	n.d.	5.0	−12.1	17.2
2′P-ADP-ribose	<0.4	8.0	−8.0	−1.3	20.5	−21.8

† From Ciulli *et al.* (2006). ITC titrations were performed in 0.1 *M* HEPES–HCl pH 7.7 at 300 K. ‡ ITC titrations were performed in 90 m*M* sodium acetate, 5 m*M* HEPES–HCl pH 4.5 at 300 K.

with the 2′-phosphate group (Ciulli *et al.*, 2006). In contrast, the results at pH 4.5 for 2′P-ADP-ribose binding differ from those of NADP$^+$ under the same conditions, which is consistent with the change of binding mode observed in the crystal structure relative to the cofactor. At pH 4.5, the Arg to Ala mutation does not affect the affinity of 2′P-ADP-ribose ($\Delta\Delta G$ < 0.4 kJ mol^{-1}; Table 3) and thus no longer discriminates against binding the ligand. These results suggest that Arg31 is not involved in the recognition of 2′P-ADP-ribose at pH 4.5. In the reversed binding mode found in the crystal this side chain is at a distance of more than 8 Å from the ligand. Although there are changes in ΔH and $T\Delta S$ of 8.0 kJ mol^{-1} for this interaction on mutation of Arg31, these changes are compensatory and can be explained as being a consequence of a change in protein structure or dynamics, rather than evidence of a direct interaction with Arg31. Conversely, the N98A mutation affected the thermodynamic parameters of 2′P-ADP-ribose binding at pH 4.5 (Table 3) in a manner that is consistent with the side chain interacting with the adenosyl group of the ligand. There were large changes in $\Delta\Delta H$ and $-T\Delta\Delta S$, although these were compensatory and thus resulted in only a small change in $\Delta\Delta G$. More importantly, these changes were remarkably different from those observed with NADP$^+$ at the same pH, further supporting the change in binding mode.

3.8. Effect of pH: rationalization of the reversed binding mode

We interpret these data as showing that the binding mode of 2′P-ADP-ribose is reversed at pH 4.5, presumably as a consequence of changes in protonation states (Fig. 3). The second pK of the 2′-phosphate group will be around 6.4 (Mas & Colman, 1984). At pH 7.7 the 2′-phosphate will be doubly charged and will interact strongly with Arg31, whereas interaction with the carboxylate side chain of Glu256, which is also negatively charged, would be unfavourable (Fig. 3*a*). In contrast, at pH 4.5 the 2′-phosphate would be present as the monoanion and Glu256 will be partially protonated. Interaction with the 2′-phosphate of the ligand will then be more favourable (Fig. 3*b*) and is observed in the crystal structure at a hydrogen-bonding distance of 2.4 Å. These changes in protonation states have triggered an otherwise unfavourable contact between a carboxylate and phosphate group and contributed significantly to the reversed binding mode observed in the crystal.

4. Conclusions

In a combined crystallographic, calorimetric and mutagenic approach, we have shown how changes in pH tune the binding of a ligand, leading to two distinct binding modes of 2′P-ADP-ribose. The crystal structure of the KPR–2′P-ADP-ribose complex is to our knowledge the first example of a reversed binding mode at the active site of a dehydrogenase. Such a novel binding mode may be possible for homologous enzymes from the same family. In the case of AHIR, a side-chain carboxylate (Asp202) binds the ribose hydroxyl groups of the cofactor in a similar way as Glu256 in KPR and could accommodate the reversed binding mode at low pH.

Targeting the cofactor-binding site of dehydrogenases such as KPR is a potential drug-design strategy for the development of novel antimicrobial compounds. This result serves as a cautionary tale for rational design using fragment-based approaches, where structural information, primarily from X-ray crystallography, is used for lead optimization. Furthermore, it stresses the importance of using complementary solution techniques such as ITC to supplement crystallography. High-resolution crystal structures of protein–ligand complexes remain the 'gold standard' for structure-based drug discovery, but due regard must be given to the conditions under which they are determined.

This work was supported by the UK Biotechnology and Biological Sciences Research Council (BBSRC) and the EU FPV HPRN-CT-2002-00244 (Viteomics). AC gratefully acknowledges Astex Therapeutics Ltd, BBSRC and the Gates Cambridge Trust for PhD funding. We thank Dr P. Andrew Karplus (Oregon State University) for the gift of 2′-monophosphoadenosine 5′-diphosphoribose, Dr Dima Y. Chirgadze for assistance with crystal optimization and X-ray data collection and Dr Glyn Williams for discussions.

References

Biou, V., Dumas, R., Cohen-Addad, C., Douce, R., Job, D. & Pebay-Peyroula, E. (1997). *EMBO J.* **16**, 3405–3415.
Bottoms, C. A., Smith, P. E. & Tanner, J. J. (2002). *Protein Sci.* **11**, 2125–2137.
Brünger, A. T., Adams, P. D., Clore, G. M., DeLano, W. L., Gros, P., Grosse-Kunstleve, R. W., Jiang, J.-S., Kuszewski, J., Nilges, M., Pannu, N. S., Read, R. J., Rice, L. M., Simonson, T. & Warren, G. L. (1998). *Acta Cryst.* D**54**, 905–921.

Burton, R. M. & Kaplan, N. O. (1963). *Arch. Biochem. Biophys.* **101**, 150–159.
Ciulli, A. & Abell, C. (2005). *Biochem. Soc. Trans.* **33**, 767–771.
Ciulli, A., Williams, G., Smith, A. G., Blundell, T. L. & Abell, C. (2006). *J. Med. Chem.* **49**, 4992–5000.
Collaborative Computational Project, Number 4 (1994). *Acta Cryst.* D**50**, 760–763.
Davis, A. M., Teague, S. J. & Kleywegt, G. J. (2003). *Angew. Chem. Int. Ed.* **42**, 2718–2736.
Denessiouk, K. A., Rantanen, V. V. & Johnson, M. S. (2001). *Proteins*, **44**, 282–291.
Holdgate, G. A. & Ward, W. H. (2005). *Drug Discov. Today*, **10**, 1543–1550.
Kleywegt, G. J. & Jones, T. A. (1998). *Acta Cryst* D**54**, 1119–1131.
Lobley, C. M., Ciulli, A., Whitney, H. M., Williams, G., Smith, A. G., Abell, C. & Blundell, T. L. (2005). *Biochemistry*, **44**, 8930–8939.
Lovell, S. C., Davis, I. W., Arendall, W. B. III, de Bakker, P. I. W., Word, J. M., Prisant, M. G., Richardson, J. S. & Richardson, D. C. (2003). *Proteins*, **50**, 437–450.
Lowry, O. H., Passonneau, J. V. & Rock, M. K. (1961). *J. Biol. Chem.* **236**, 2756–2759.
McRee, D. E. (1999). *J. Struct. Biol.* **125**, 156–165.
Mas, M. T. & Colman, R. F. (1984). *Biochemistry*, **23**, 1675–1683.
Matak-Vinkovic, D., Vinkovic, M., Saldanha, S. A., Ashurst, J. L., von Delft, F., Inoue, T., Miguel, R. N., Smith, A. G., Blundell, T. L. & Abell, C. (2001). *Biochemistry*, **40**, 14493–14500.
Murshudov, G. N., Vagin, A. A. & Dodson, E. J. (1997). *Acta Cryst.* D**53**, 240–255.
Murzin, A. G., Brenner, S. E., Hubbard, T. & Chothia, C. (1995). *J. Mol. Biol.* **247**, 536–540.
Navaza, J. (1994). *Acta Cryst.* A**50**, 157–163.
Navaza, J. (2001). *Acta Cryst.* D**57**, 1367–1372.
Otwinowski, Z. & Minor, W. (1997). *Methods Enzymol.* **276**, 307–326.
Primerano, D. A. & Burns, R. O. (1983). *J. Bacteriol.* **153**, 259–269.
Schüttelkopf, A. W. & van Aalten, D. M. F. (2004). *Acta Cryst.* D**60**, 1355–1363.
Thomazeau, K., Dumas, R., Halgand, F., Forest, E., Douce, R. & Biou, V. (2000). *Acta Cryst.* D**56**, 389–397.
Turnbull, W. B. & Daranas, A. H. (2003). *J. Am. Chem. Soc.* **125**, 14859–14866.
Ward, W. H. & Holdgate, G. A. (2001). *Prog. Med. Chem.* **38**, 309–376.
Wiseman, T., Williston, S., Brandts, J. F. & Lin, L. N. (1989). *Anal. Biochem.* **179**, 131–137.
Zheng, R. & Blanchard, J. S. (2000*a*). *Biochemistry*, **39**, 3708–3717.
Zheng, R. & Blanchard, J. S. (2000*b*). *Biochemistry*, **39**, 16244–16251.
Zheng, R. & Blanchard, J. S. (2003). *Biochemistry*, **42**, 11289–11296.